



**HAL**  
open science

## Effects of functional groups and anion size on the charging mechanisms in layered electrode materials

Kui Xu, Céline Merlet, Zifeng Lin, Hui Shao, Pierre-Louis Taberna, Ling Miao, Jianjun Jiang, Jixin Zhu, Patrice Simon

► **To cite this version:**

Kui Xu, Céline Merlet, Zifeng Lin, Hui Shao, Pierre-Louis Taberna, et al.. Effects of functional groups and anion size on the charging mechanisms in layered electrode materials. *Energy Storage Materials*, 2020, 10.1016/j.ensm.2020.08.030 . hal-02933837

**HAL Id: hal-02933837**

**<https://hal.science/hal-02933837>**

Submitted on 8 Sep 2020

**HAL** is a multi-disciplinary open access archive for the deposit and dissemination of scientific research documents, whether they are published or not. The documents may come from teaching and research institutions in France or abroad, or from public or private research centers.

L'archive ouverte pluridisciplinaire **HAL**, est destinée au dépôt et à la diffusion de documents scientifiques de niveau recherche, publiés ou non, émanant des établissements d'enseignement et de recherche français ou étrangers, des laboratoires publics ou privés.

# Effects of functional groups and anion size on the charging mechanisms in layered electrode materials

Kui Xu,<sup>a,b,c</sup> Céline Merlet,<sup>b,c,\*</sup> Zifeng Lin,<sup>d</sup> Hui Shao,<sup>b,c</sup> Pierre-Louis Taberna,<sup>b,c</sup> Ling Miao,<sup>e</sup> Jianjun Jiang,<sup>e</sup> Jixin Zhu,<sup>a</sup> Patrice Simon<sup>b,c,f,\*</sup>

<sup>a</sup> Key Laboratory of Flexible Electronics (KLOFE) & Institute of Advanced Materials (IAM), Jiangsu National Synergetic Innovation Center for Advanced Materials (SICAM), Nanjing Tech University (NanjingTech), 30 South Puzhu Road, Nanjing 211816, P. R. China

<sup>b</sup> Université de Toulouse, CNRS, CIRIMAT, 118, route de Narbonne 31062 Toulouse cedex 9, France

<sup>c</sup> Réseau sur le Stockage Electrochimique de l'Energie (RS2E), Federation de Recherche CNRS 3459, 33 rue Saint Leu, 80039 Amiens, France

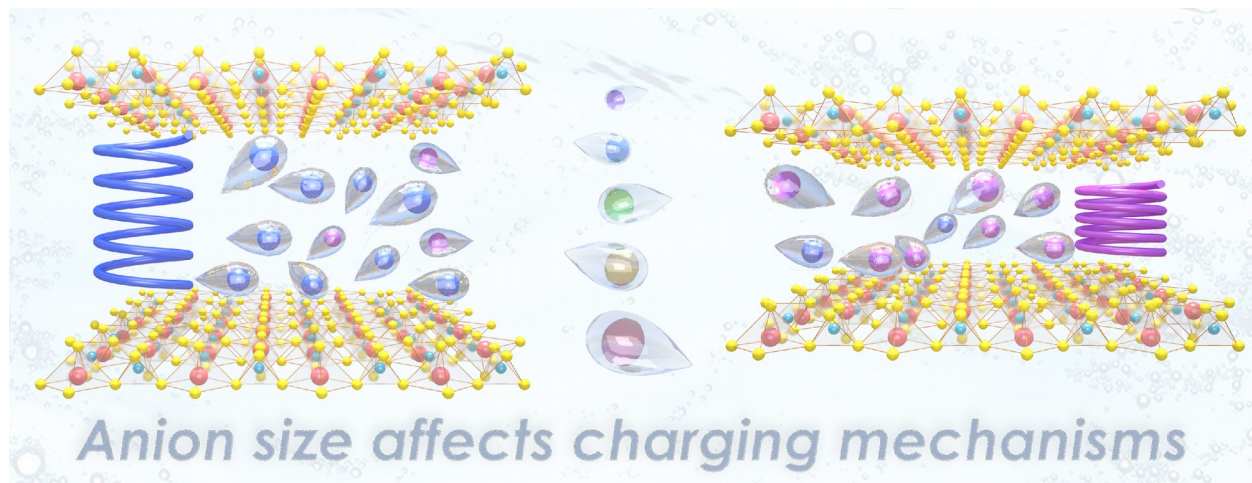
<sup>d</sup> College of Materials Science and Engineering, Sichuan University, No.24 South Section 1, Yihuan Road, Chengdu 610065, P. R. China

<sup>e</sup> School of Optical and Electronic Information, Huazhong University of Science and Technology, Wuhan, Hubei 430074, P. R. China

<sup>f</sup> Institut Universitaire de France, 1, Rue des Ecoles, 75005 Paris, France

**E-mail:** [merlet@chimie.ups-tlse.fr](mailto:merlet@chimie.ups-tlse.fr), [simon@chimie.ups-tlse.fr](mailto:simon@chimie.ups-tlse.fr)

## TOC



## Keywords

MXenes, ionic liquids, molecular simulations, volume expansion/contraction, charge storage mechanisms

## Highlights

- We have conducted molecular simulations on 20 model supercapacitors systems based on graphene or MXene electrodes, with different functional groups, and 5 neat ionic liquids, with different anions.
- When charging negatively, the electrodes expand and no major dependence on the anion type is observed. When charging positively, the volume changes are more complex.
- Volume changes are generally very well correlated with the quantities of adsorbed ions, except for the largest anions for which ion reorientations affect the interlayer spacing.
- We demonstrate that the charging mechanisms are largely correlated with the anion sizes and the surface charge of the electrode material in the uncharged state.

## Abstract

We report on an extensive molecular simulations study about the influence of the nature of functional groups and anion size on the charging mechanisms and volume expansion/contraction in layered materials used as electrodes for energy storage applications. The study of the electrochemical behavior of graphene and  $\text{Ti}_3\text{C}_2$  MXene (with three different functional groups) in five ionic liquids shows that the electrodes expand when charged negatively and no major dependence on the anion type is observed. When the electrode is positively charged, the volume changes are more complex and no specific trend could be observed depending on the anion size. The volume changes are in most cases, very well explained by the quantities of adsorbed ions. In specific cases, e.g., for  $\text{FSI}^-$  and  $\text{TFSI}^-$  anions, the reorientation of the ions can also affect the interlayer volume. We demonstrate that the charging mechanisms are changing consistently with the anion sizes and are largely correlated with the surface charge of the electrode material in the neutral state.

## 1. Introduction

Electrical energy storage (EES) has attracted huge attention from the scientific community in the past decades due to its widespread usage and irreplaceable function in our daily life.<sup>1</sup> Batteries have played a dominant role for years due to their high performance and moderate price. However, supercapacitors, also known as electrical double-layer capacitors, have played an increasingly important role in the EES market and research field. Supercapacitors show their superiority in fast energy delivery or harvesting but suffer from moderate energy densities.<sup>2</sup> It is therefore essential to seek ways to increase their energy density without compromising their power density.

Like batteries, the electrochemical performance of a supercapacitor device is mainly determined by its active components, i.e., the electrodes and electrolyte. On the electrode side, recent studies have demonstrated that transition metal-based, low-dimensional systems, could be promising excellent electrode materials for EES, due to their superior electronic properties, multiple oxidation states, spin states, etc.<sup>3-6</sup> Two-dimensional transition metal carbides and

nitrides, also called MXenes, are one of the typical representatives of these transition metal-based low dimensional systems.<sup>7,8</sup> Due to the relatively weak attractive interaction between MXene layers and the existence of hydrophilic groups on the layer surface inherent to the synthesis process, the electrolyte ions can spontaneously intercalate into MXenes, which significantly enhances the electrochemical performance, leading to high gravimetric and volumetric capacitances along with remarkable cyclability.<sup>9-12</sup> Compared to some other conventional pseudocapacitive materials, including transition metal oxides, conductive polymer, and redox-active organic molecules, MXene electrodes not only exhibit a promising capacitance but also have much better cyclability.<sup>13</sup>

Selecting an appropriate electrode/electrolyte system is critical to achieving a high energy density EES device. Extensive experimental work has focused on understanding the charging mechanisms for MXenes combined with various electrolytes. In neat ionic liquids or neutral and alkaline aqueous solutions, MXenes mainly exhibit double layer capacitance resulting from electrostatic adsorption. In aqueous H<sub>2</sub>SO<sub>4</sub>, MXenes show a pseudocapacitive behavior, due to the fast surface reversible redox reactions of titanium.<sup>11,14,15</sup> In lithium or sodium-based organic electrolytes, MXenes show intercalation pseudocapacitance.<sup>10,16</sup> Wang *et al.* observed a drastic influence of the solvent on the pseudocapacitive charge storage of the Ti<sub>3</sub>C<sub>2</sub> MXene material.<sup>17</sup> With lithium-based electrolytes and Ti<sub>3</sub>C<sub>2</sub>, one can obtain twice larger charge storage when using carbonate solvents compared with nitrile- or sulfoxide-based solvents. Overall, the chemical nature of the electrolyte ions and the solvent has an important effect on the molecules/ions arrangement in Ti<sub>3</sub>C<sub>2</sub>, which is in direct correlation with the total charge storage ability.

Understanding the charge storage mechanisms and designing the right combination of electrode and electrolyte is therefore essential and meaningful. However, due to the large number of possible MXene/electrolyte associations, and the technical difficulty, as well as the cost, of synthesizing some MXenes, a systematic experimental exploration of the charging mechanism and capacitive performance of the MXene family would be very costly and time-consuming.<sup>18</sup> Nowadays, among different computational methods, molecular dynamics (MD)

simulations are playing a pivotal role in investigating mechanisms in-depth and designing supercapacitors with improved capacitive performance in a more effective way.<sup>19-21</sup>

MD simulations can provide detailed and realistic ionic diffusion coefficients, intercalation and electrode structural information of such 2D layered materials and systems. Muckley *et al.* report the use of MD simulations for exploring the driving force inducing the volumetric changes during hydration and dehydration cycles.<sup>22</sup> Osti *et al.* demonstrated that the presence of  $K^+$  ions could reduce the self-diffusion of water molecules and enhance the stability of hydrated MXene, in agreement with their experimental results.<sup>23</sup> The dynamical structural response of MXenes to the ion intercalation during the electrochemical process is crucial, Berdiyrov *et al.* observed an increase and a decrease of the MXene interlayer distance when intercalating anions and cations, respectively.<sup>24</sup> Xu *et al.* employed a multi-layer MXene / ionic liquid simulation system with flexible interlayer spacing to obtain an atomic scale image of the molecular changes occurring during charge and discharge.<sup>25</sup> These simulations reproduce the trend observed in electrochemical and X-ray diffraction experiments<sup>26,27</sup> and allow them to propose mechanisms for the volume expansion, at negative polarization, and contraction, at positive polarization.

In this work, we conduct molecular dynamics simulations of a range of model supercapacitors based on layered materials and neat ionic liquid electrolytes. On the electrode side, graphene and  $Ti_3C_2$  MXene with three functional groups ( $Ti_3C_2F_2$ ,  $Ti_3C_2O_2$ ,  $Ti_3C_2(OH)_2$ ) are selected for investigating the effect of the nature of the electrode material and functional groups on charge storage mechanism. On the electrolyte side, we vary the anion type and analyze the changes incurred on the relative volume expansion. The results are then interpreted through a detailed description of the charging mechanisms, ion reorientations, and free energies.

## 2. Methods

The model supercapacitors consist of two electrodes made of 4 layers of graphene or MXene immersed in a pure ionic liquid (see Figure 1). All supercapacitors are symmetrical, i.e., the positive and negative electrode materials are identical, and the spacing between layers,  $d$ , is

allowed to vary while the atomic positions within a given layer are rigid. Four different types of electrode materials are investigated: graphene,  $\text{Ti}_3\text{C}_2\text{F}_2$ ,  $\text{Ti}_3\text{C}_2\text{O}_2$ , and  $\text{Ti}_3\text{C}_2(\text{OH})_2$ . The carbon atoms of graphene are neutral in the initial state and the atomic charges for the MXene materials are taken from the literature.<sup>22,28</sup> The partial charges of the MXene atoms balance each other so that the electrodes are overall neutral in the uncharged state. All force field and structural parameters for the simulations of the electrode materials are taken from Xu *et al.*<sup>25</sup> Five ionic liquids with a common cation (1-ethyl-3-methylimidazolium, EMIM<sup>+</sup>) and anions of different sizes (see Table 1) were investigated. The various anions studied are: chloride (Cl<sup>-</sup>), tetrafluoroborate (BF<sub>4</sub><sup>-</sup>), trifluoromethanesulfonate (OTF<sup>-</sup>), bis(fluorosulfonyl)imide (FSI<sup>-</sup>) and bis(trifluoromethane-sulfonyl)imide (TFSI<sup>-</sup>). For all the ions, the OPLS-AA force field was used.<sup>29-31</sup> The structures of the ions and electrodes studied here are shown in Figure 2.

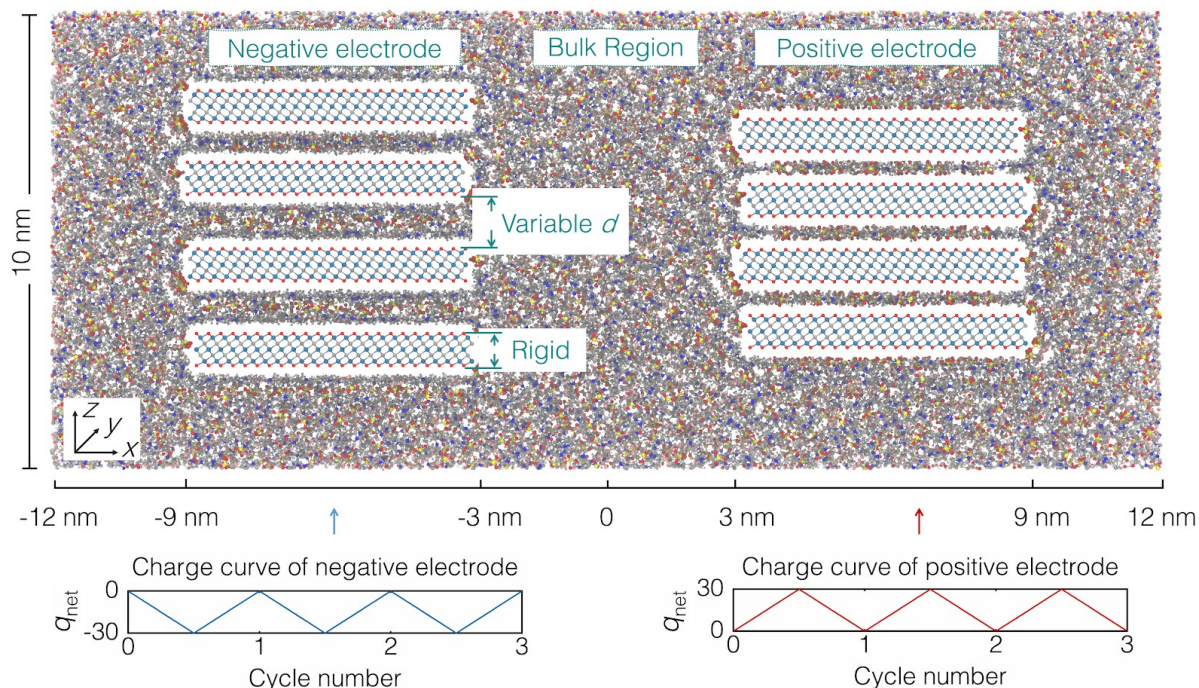


Figure 1: Snapshot of a typical MXene based simulation box. For the MXene electrodes, the oxygen, titanium, and carbon atoms are in red, blue, and grey, respectively. The electrodes are fully immersed in the electrolyte (EMIM-TFSI is represented here). Each MXene layer has rigid internal positions but the layers can move with respect to each other. The total charge on each electrode varies between 0 and  $\pm 30.0 \mu\text{C}\cdot\text{cm}^{-2}$  along a cycle.

All the simulations are done in the NVT ensemble using the LAMMPS software.<sup>33</sup> The temperature is set to 450 K and the timestep is 1 fs. This temperature was set to compensate for the slow dynamics observed when using the chosen force field. These slow dynamics are due to the use of full charges of  $\pm 1e$  for the ions instead of the  $\pm 0.8e$  sometimes proposed to take into account the effective charge screening in concentrated electrolytes.<sup>34-37</sup> Here the use of full charges is preferred to avoid any effect of a charge scaling on the number of adsorbed ions at a given charged state. While this temperature might seem high, experiments show that all the ionic liquids studied here are stable at this temperature.<sup>38-41</sup> The long-range electrostatic interactions are calculated via the particle-particle particle-mesh Ewald scheme (pppm), which is a commonly used Fourier-based Ewald summation method. A cutoff is set to 1.0 nm for the van der Waals interactions.

Ion	EMIM <sup>+</sup>	Cl <sup>-</sup>	BF <sub>4</sub> <sup>-</sup>	OTF <sup>-</sup>	FSI <sup>-</sup>	TFSI <sup>-</sup>
Ion volume (nm <sup>3</sup> )	0.194	0.049	0.089	0.141	0.176	0.239

Table 1: Ion volumes used in the calculation of the total ionic volume for the ions adsorbed inside the electrodes, estimated based on the Connolly surface method.<sup>32</sup>

To study the volume changes upon charging and discharging, we follow an approach which allows us to mimic galvanostatic cycling experiments. All systems are first equilibrated with a null charge on the electrodes for 1.8 ns. The systems then undergo three charging/discharging cycles of 0.3 ns each. The charge current density is equal to 200 kA.cm<sup>-2</sup>. Although it is orders of magnitude higher than the values commonly used experimentally, it has been proven that it could lead to a realistic behavior<sup>42</sup>. In particular, Xu et al. have shown that with these cycling rates, longer simulations holding the system at the maximum charged state do not lead to significant changes in the interlayer spacing and that additional cycles do not lead to increasing deviations from the first three<sup>25</sup>. This fast charging/discharging results from the much smaller system sizes considered in simulations, in the order of nanometers, compared to

experiments, in the order of micrometers or more. It is worth noting though that the surface used here to calculate the current density is the specific surface area of MXene, which is probably different from the foot print area in experimental electrodes. In practice, a partial charge, evolving linearly with time, is applied to every electrode atom. The charge density on each electrode surface is equal to  $30.0 \mu\text{C}\cdot\text{cm}^{-2}$  at the maximum charged state. This corresponds to a partial charge added on each atom of 0.016 e, 0.021 e, 0.021 e, and 0.016 e for graphene,  $\text{Ti}_3\text{C}_2\text{F}_2$ ,  $\text{Ti}_3\text{C}_2\text{O}_2$ , and  $\text{Ti}_3\text{C}_2(\text{OH})_2$ , respectively. An example of partial atomic charges in the zero and maximum charged states is given in Figure S1. The difference in net partial charge between the electrodes originates from the different numbers of atoms in each electrode layer. The resulting surface charge density is consistent with experimental results, for example from Wang *et al.*<sup>17</sup>, which show values in the  $30\text{-}90 \mu\text{C}\cdot\text{cm}^{-2}$  range for the Li-TFSI salt in various solvents (0.37 e per  $\text{Ti}_3\text{C}_2$  unit for acetonitrile and 0.93 e per  $\text{Ti}_3\text{C}_2$  unit for propylene carbonate). In order to ensure reliable statistics, every simulation is repeated three times with independent initial configurations. Figure S2 shows an example of standard errors calculated for the net ionic charge in the interlayer spacing along the three charge/discharge cycles, averaged over the three independent simulations. The errors made on this collective quantity (one value per electrode per configuration) are satisfying for the purpose of this work. A more detailed discussion of the simulation process and its validity is available in Xu *et al.*<sup>42</sup>

While a number of works have shown that using a constant potential approach, i.e. allowing the charge on the atoms to fluctuate in response to the nearby electrolyte, is a more realistic way to model carbon-based supercapacitors,<sup>43-45</sup> here the choice was made to use constant charge simulations. The current system is fundamentally different from the carbon-based systems used in previously reported studies as the electrodes contain a large number of heteroatoms (Ti, O, F). In the constant potential approach, all atomic charges behave in the same way which is improbable in the electrode materials investigated here. While the different atom types are characterized by different positions in the electrode material and different Lennard-Jones parameters, corresponding to short-range Van der Waals forces, the fluctuations of the charges would be treated in an equivalent manner for all atom types. Moreover, the systems simulated here are represented using all-atom models and the electrodes are fully

immersed in the electrolyte, necessitating large simulation boxes containing between 80,000 and 100,000 atoms, making constant potential calculations computationally intractable. We have thus preferred an approach in which small partial are added on the *ab initio* determined values.<sup>22,28</sup> This approach, corresponding to a revisited constant charge method with atomic charges distributed non uniformly and increasing linearly with time, is consistent with experimental results from EELS and XANES showing that the oxidation state of MXene atoms only changes weakly upon charging.<sup>14,17</sup> In addition, the simulations do not show any sign of problematic charging dynamics such as a large rise in temperature as was observed in some of the constant charge simulations reported previously.<sup>43</sup> These observations along with the multiple properties in good agreement with experimental results (surface charges at maximum charged state, interlayer spacing at 0V and its variation with applied potential) make us confident that the constant charge approach is suitable for such a study. Nevertheless, it is worth noting that a more realistic approach would include a semi-metallic and differentiated behavior for the different MXene atoms, allowing for charge fluctuations responsive to the surrounding electrolyte. This is not something feasible with current simulation techniques. If such a simulation approach becomes available in the future, it would be interesting to check how such properties affect the results. Local ion densities and orientations could for example be modified by local and fluctuating charge heterogeneities. The effects of such local quantities on the properties discussed here are expected to be limited according to the above comments.

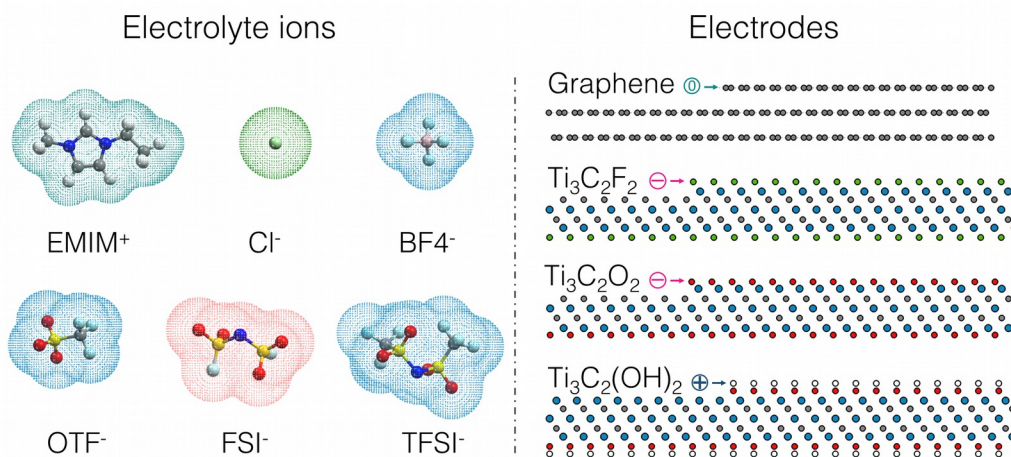


Figure 2: Chemical structures of the electrolyte ions and electrodes studied in this work.

Additional simulations of the bulk electrolytes were conducted to evaluate diffusion coefficients of the various species in the absence of electrodes. The simulations were done with 7440, 6552, 5418, 4878, 3996 ion pairs (for EMIM-Cl, EMIM-BF<sub>4</sub>, EMIM-OTF, EMIM-FSI, EMIM-TFSI, respectively), and consisted in an equilibration of 1.0 ns in the NPT ensemble at 1 bar and 450 K followed by a production run of 1.0 ns in the NVT ensemble at the same temperature. All other parameters are identical to the model supercapacitors simulations.

### 3. Results and discussion

#### 3.1 Relative volume changes

The first property we examine is the relative volume expansion/contraction which can be quantitatively measured experimentally. In our simulations, this expansion/contraction can be calculated from the interlayer spacing which is monitored during the charging/discharging process. The relative volume changes averaged over three cycles for all the systems are shown in Figure 3. For all electrode materials and electrolytes, the electrode expands when the electrode is charged negatively and no major dependence on the anion type is observed. Since the cation is the same for all the electrolytes, we can expect that the effect of the anion type on the negative electrode side is limited.

It is worth noting that while the relative expansion is very similar for all materials, the initial equilibrium interlayer spacing ( $d_0$ ) can be different (see Figure 4). For the graphene electrode in contact with the largest ions (EMIM-TFSI), the initial equilibrium interlayer spacing has a value of 1.08 nm. For smaller anions, the initial equilibrium interlayer spacing is slightly smaller, around 1.03 - 1.05 nm. For the MXene electrodes with different functional groups, the initial equilibrium interlayer spacings show a similar trend:  $d_0$  first increases when the anion size increases, reaches a maximum for the case of EMIM-OTF, and then decreases while the anion size increases. The values obtained here for MXene materials immersed in EMIM-TFSI are in good agreement with the X-ray diffraction results of Liu *et al.*<sup>27</sup> which showed a peak at  $2\theta$

equal to  $8.5^\circ$  at 0 V, corresponding to a c-lattice parameter of 2.08 nm and thus an interlayer spacing close to 1 nm.

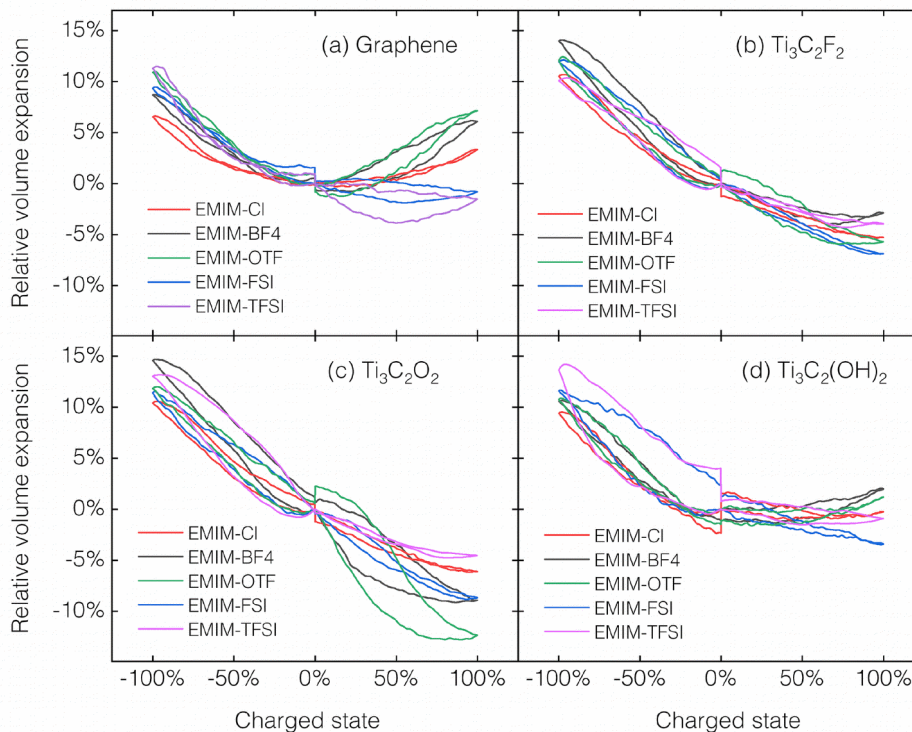


Figure 3: Relative volume expansion/contraction for all the systems studied in this work.

Going back to the relative volume variations, on the positive electrode side, the change is more complex and depends both on the anion type and on the electrode material. For the graphene electrode, surprisingly, the smallest anions ( $\text{Cl}^-$ ,  $\text{BF}_4^-$ ,  $\text{OTF}^-$ ) lead to a volume expansion while the largest anions ( $\text{FSI}^-$  and  $\text{TFSI}^-$ ) cause a volume contraction. For the  $\text{Ti}_3\text{C}_2\text{O}_2$  MXene electrode, all electrolytes induce a volume contraction but with different magnitudes. When changing the MXene surface groups, that is for  $\text{Ti}_3\text{C}_2\text{F}_2$  and  $\text{Ti}_3\text{C}_2(\text{OH})_2$ , a similar trend is observed for all anions. None of the electrode materials show a monotonous variation with the anion size.

To the best of our knowledge, there is no extensive reported study on the understanding of how the nature of the electrode and electrolyte impacts the volume expansion/contraction in two-dimensional layered materials. For the graphene electrode case,

we compare our results with a series of experimental porous carbons and carbon membrane systems in contact with pure ionic liquids or ionic liquid - acetonitrile mixtures.<sup>46-48</sup> Using *in situ* electrochemical dilatometry, Kaasik *et al.*<sup>49</sup> and Hantel *et al.*<sup>48</sup> observed relative electrode expansions during both negative and positive charging of different carbons systems (carbide-derived carbons, YP17, BP2000 and MM) in pure EMIM-BF<sub>4</sub>, which is qualitatively consistent with the EMIM-BF<sub>4</sub> simulation results. For the MXene electrodes, our results are in good agreement with the *in situ* experiments described by Jackel *et al.*<sup>26</sup> and Lin *et al.*<sup>27</sup> Indeed, for the EMIM-TFSI electrolyte, X-ray diffraction and electrochemical dilatometry studies have both shown a volume expansion when charging negatively and a volume contraction when charging positively. The relative changes between uncharged and charged states are usually larger for simulations compared to experiments, which is likely due to the difference in charge distribution across the electrode atoms as well as the concentration of surface functional groups and the non uniform grain size. In addition, for dilatometry experiments, part of the volume variation could be buffered due to the dead volume between the grains of active materials. Overall, the agreement is satisfying, and we move forward to the interpretation of the volumetric changes observed.

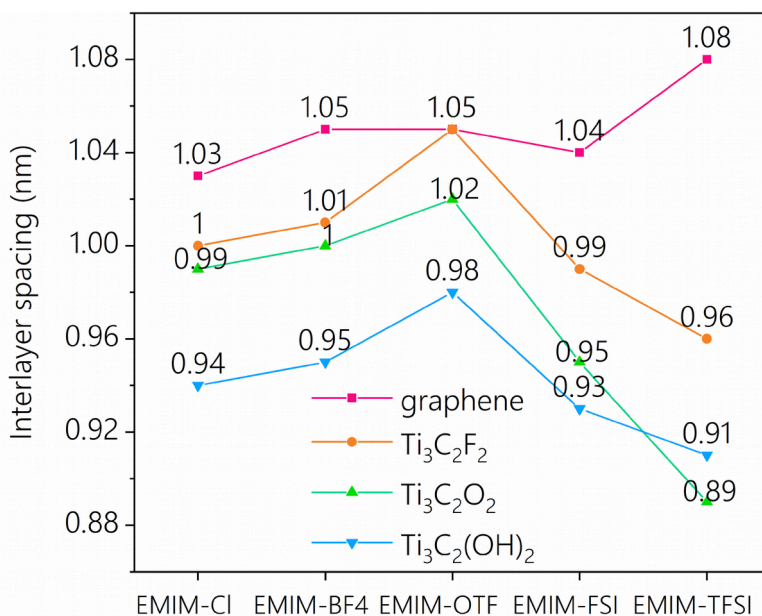


Figure 4: Initial equilibrium interlayer spacing of various electrode materials and electrolytes.

### 3.2 Ionic number changes

In this section, we compare the volume changes with the number of ions present in the interlayer region at various charge states. Figures 5 and S3 show the evolution of the number of ions inside the electrodes during the charging/discharging processes of graphene and MXenes materials. We first focus on the graphene electrodes. At the negative electrode, cations are always involved in the charge storage although the total number of ions entering or leaving the interlayer region seems to decrease with the increase in anion size. For small anion sizes, anionic populations changes show amplitudes similar to the cationic ones but for large anion sizes (larger than OTF<sup>-</sup>), it seems that the number of anions is almost constant. Overall, the picture seems to be consistent with the change in volume (expansion at the negative electrode) as either smaller anions are replaced by larger cations or cations enter the electrode at a constant number of anions. On the positive electrode side, for EMIM-Cl, EMIM-BF<sub>4</sub>, and EMIM-OTF, the anions are mostly responsible for the charge storage since the number of cations is nearly constant. This is consistent with a volume expansion for these systems. For EMIM-FSI and EMIM-TFSI, there are fewer anions going in and out of the electrodes and the charge is mainly balanced by cation deintercalation. As a result, a volume contraction is observed. Overall, it seems that the smaller the anion, the more it contributes to the charge storage and to the change in volume. For bigger anions, the anion population change is smaller and impacts the volume less.

For the Ti<sub>3</sub>C<sub>2</sub>F<sub>2</sub> electrode material, ion numbers show a similar behavior as for graphene at the negative polarization. On the positive electrode side, however, cations are leaving the electrode even for the smallest anion sizes, which explains the volume contraction observed in all electrolytes. Similar comments can be made for the Ti<sub>3</sub>C<sub>2</sub>O<sub>2</sub> and Ti<sub>3</sub>C<sub>2</sub>(OH)<sub>2</sub> electrode materials. While all electrode materials show specific behaviors, we note that graphene and Ti<sub>3</sub>C<sub>2</sub>(OH)<sub>2</sub> on the one hand and Ti<sub>3</sub>C<sub>2</sub>O<sub>2</sub> and Ti<sub>3</sub>C<sub>2</sub>F<sub>2</sub> on the other hand, are related. This may be due to the presence of similar initial charges on those systems, with graphene being neutral and -OH groups being close to neutral while -F and =O are charged more negatively. It is interesting to note that while the behavior when charging is different between these types of surface functional groups, the number of adsorbed ions in the uncharged state is more affected

by the electrolyte nature than by the nature of the functional groups. It should be noted that the initial partial charges on the MXenes atoms are such that the electrodes are overall neutral in the uncharged state (detailed partial charge information can be found in Xu *et al.*<sup>25</sup>).

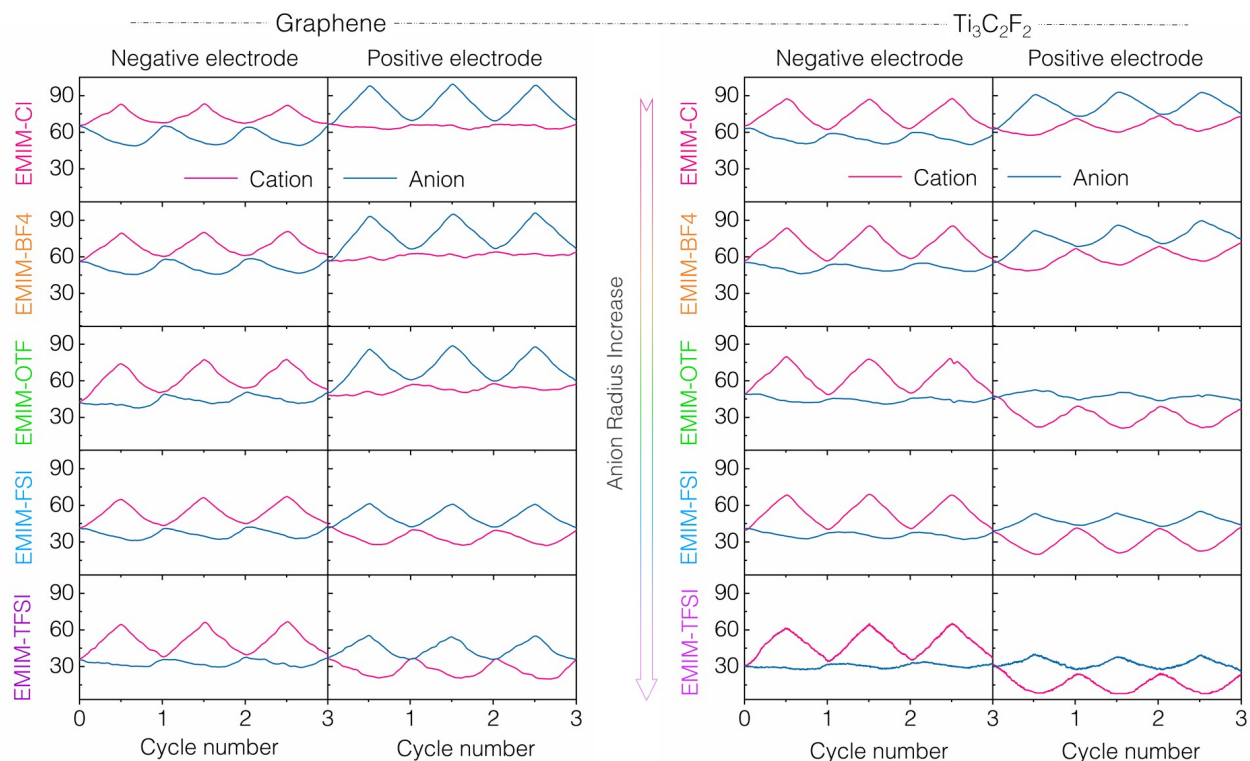


Figure 5: Evolution of the ion numbers in the graphene and  $\text{Ti}_3\text{C}_2\text{F}_2$  electrodes during charging and discharging.

### 3.3 Comparison of ionic and geometrical volumes

Going beyond the ion numbers, it is possible to calculate the actual ionic volumes occupied by the electrolyte in the interlayer spacing and compare those to the electrode interlayer spacing volumes. Figures 6, S4, S5, and S6 show a comparison of the ionic volumes and interlayer volumes. In most cases, there is a qualitative agreement, if not quantitative, between those values. Discrepancies observed between these two numbers can be due to statistical errors in estimating the number of ions in the interlayer region at a given state as well as small errors made by assuming that all atoms of an ion are in the electrode if the center of mass of this ion is in the electrode.

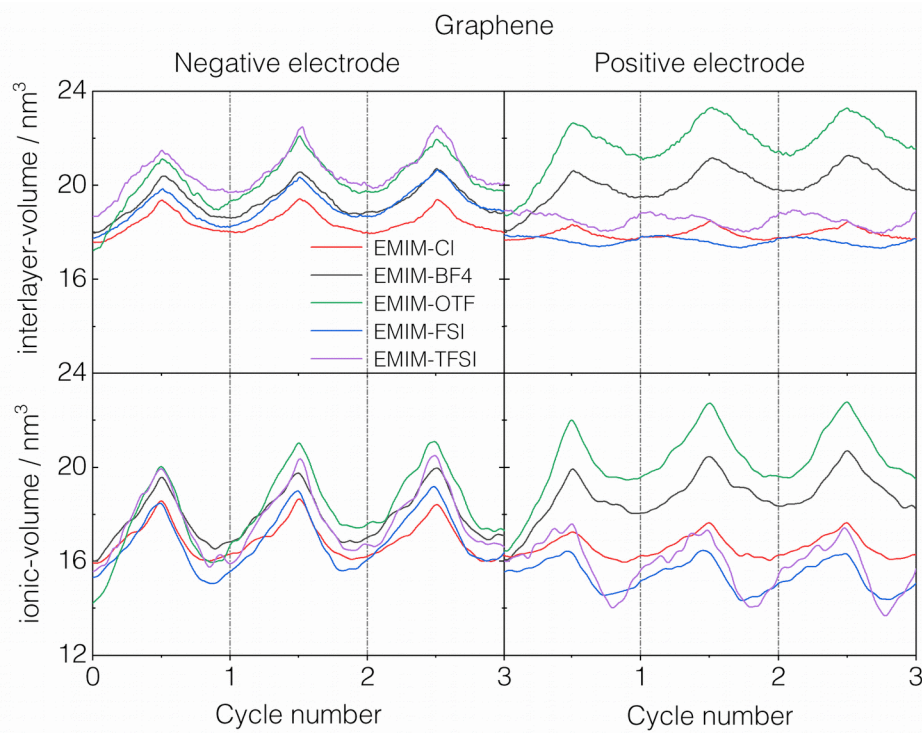


Figure 6: Comparison between the interlayer volumes calculated using the interlayer distances and the ionic volumes for the graphene electrodes.

The cases of EMIM-FSI and EMIM-TFSI in contact with graphene electrodes are, at first sight, not so satisfactory since the interlayer volume is almost constant while the number of ions is changing upon charging and discharging. Actually, in these systems, a reorientation of the ions is observed, which we characterize through orientation distribution functions in Figure 7(a) for the neutral state, and as a function of the polarization in 7(b) and 7(c). These plots give the probability of finding the molecules at various angles in the interlayer region. The orientation distribution functions for  $\text{EMIM}^+$  and  $\text{FSI}^-$  show that, in the neutral state, both cations and anions lie preferentially parallel to the layer surface in such a slit interlayer. During charging and discharging, we observe a continuous cyclic evolution of the orientation of cations and anions at both positive and negative sides. For  $\text{FSI}^-$  at the positive electrode, the probability for the parallel orientation ( $\theta \sim 90^\circ$ ) is increasing when charging, and decreasing when discharging, as shown in Figure 7(b). A reverse trend is seen at the negative electrode. For  $\text{EMIM}^+$ , there is a

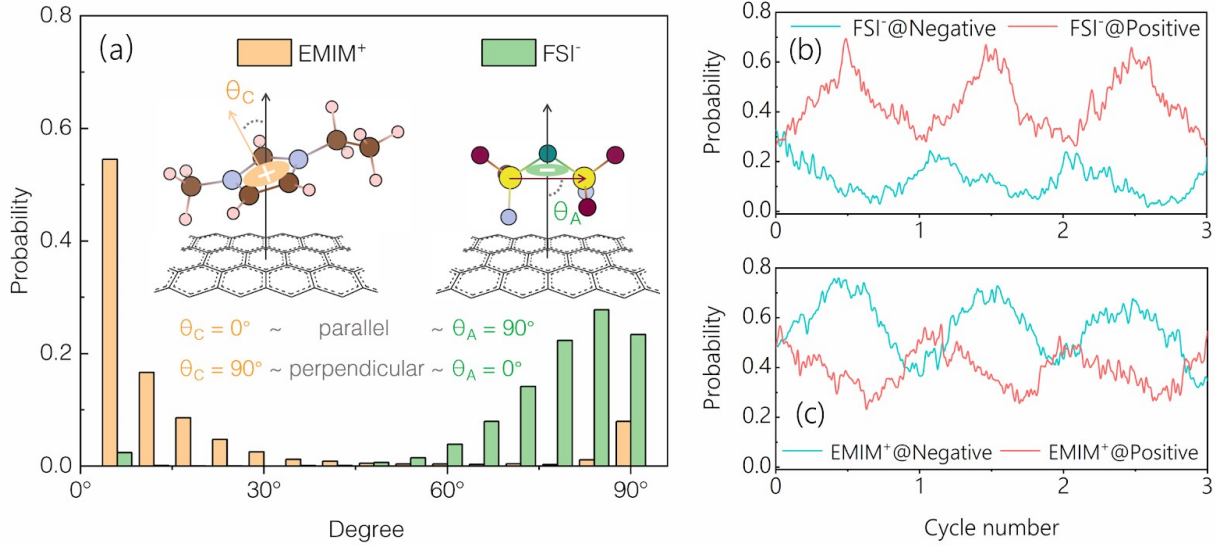


Figure 7: (a) Orientation distribution functions for EMIM<sup>+</sup> and FSI<sup>-</sup> confined in the graphene interlayer spacing in the neutral state. For EMIM<sup>+</sup>,  $\theta \sim 0^\circ$  corresponds to the imidazolium ring parallel to the carbon surface and  $\theta \sim 90^\circ$  corresponds to the imidazolium perpendicular to the carbon surface. For FSI<sup>-</sup>,  $90^\circ$  corresponds to the S-S vector parallel to the surface and  $0^\circ$  corresponds to the S-S vector perpendicular to the surface. The insets illustrate the definition of the angle. (b) Probability of the  $90^\circ$  angle for FSI<sup>-</sup> as a function of cycle number. (c) Same for the  $0^\circ$  angle for EMIM<sup>+</sup>.

similar increasing trend on the counter-charged electrode and a decreasing trend on the co-charged electrode, as shown in Figure 7(c). This continuous reorientation of the ions is thought to be one of the main origins of the deviation of the interlayer and ionic volumes, especially for the EMIM-FSI and EMIM-TFSI cases. While we focus here on specific angles, i.e. the most probable ones, the full orientation distribution functions are given in Figures S7 and S8. For the MXenes based electrodes, similar trends of orientation change are observed with all three kinds of functional groups. It is worth noting that reorientations are also observed for OTF<sup>-</sup> in EMIM-OTF (results not shown for brevity) but these do not lead to major discrepancies between ionic volume and interlayer volume, the effect of these reorientations thus seems negligible compared to the numbers of adsorbed ions in this case.

### 3.4 Charge storage mechanisms

We have illustrated in the previous section that the ionic volumes and the interlayer volumes are tightly correlated. We now turn to a detailed analysis of the charge storage mechanisms and how they are affected by the anion and electrode types. When a charge, or a potential, is applied to the electrodes, several events can occur. Forse *et al.* have proposed to classify these events as counter-ions entering the electrode, counter-ions going in while co-ions are going out, co-ions leaving the electrode<sup>50</sup>. We refer to these mechanisms as intercalation, exchange, and deintercalation. In the molecular simulations, we have access to counter-ions and co-ions numbers, and we can thus estimate the proportion of each mechanism happening in the studied systems. Figure S9 shows such proportions for all the systems studied in this work. Because we consider that ions contribute to ion exchange before contributing to intercalation and deintercalation, it is not possible to observe intercalation (of counter-ions) and deintercalation (of co-ions) at the same time. As such, a simplified way of looking at these mechanisms is to consider only the intercalation and deintercalation without considering the ion exchange.

Figure 8 shows the proportions of intercalation and deintercalation for all systems studied here. While we focus on the maximum charged state, and do not provide a detailed evolution with time as proposed in previous works,<sup>51-52</sup> the ratio between intercalation and deintercalation is not expected to change much along the trajectory following the linear ion numbers profiles, in phase with the imposed cycling, observed in Figures 5 and S3. On the negative electrode side, intercalation is always the predominant mechanism. When the anion size increases, the contribution of intercalation to the total charge increases. This is quite intuitive as larger anions will be less mobile and as such, the cations, i.e. the counter-ions in this case, will be more involved in the charge storing. All electrode materials show a similar trend, but the intercalation is consistently more important for  $\text{Ti}_3\text{C}_2\text{O}_2$  and  $\text{Ti}_3\text{C}_2\text{F}_2$  compared to graphene and  $\text{Ti}_3\text{C}_2(\text{OH})_2$ . The negative charge on the surface groups is larger for -F and =O, which generates an attractive force on the cations in these systems. On the positive side, a reverse trend is observed with anion size, again consistent with the anions, counter-ions in this electrode, becoming less mobile as their size increases and facing a higher energy barrier when

entering into the  $\text{Ti}_3\text{C}_2\text{O}_2$  and  $\text{Ti}_3\text{C}_2\text{F}_2$  layer.  $\text{Ti}_3\text{C}_2\text{O}_2$  and  $\text{Ti}_3\text{C}_2\text{F}_2$  are the only two electrodes materials showing a predominant deintercalation for the largest anion sizes.



Figure 8: Proportions of intercalation and deintercalation at the maximum charged state for all the electrode materials and electrolytes studied in this work.

We have done additional calculations on the bulk electrolytes to explore the effect of the ion mobility further. Diffusion coefficients calculated for the anions and cations are given in Figure S10. For all electrolytes, cations diffuse faster than anions, in agreement with a number of experimental and theoretical studies.<sup>53-55</sup> This might explain why intercalation of cations is always predominant on the negative electrode side but the picture is overall much more complicated. In particular, neither the relative difference between anions and cations nor the diffusion coefficients themselves follow a monotonous trend with the anion size. So no direct correlation between the ion mobility and the charging mechanisms observed can be made.

Characterizing the ion mobility in confinement and while charging and discharging would be very challenging here as it changes with the state of charge. Actually, migration and diffusion are two different aspects of ion mobility and trying to relate both in a given system is out of the scope of this article.

### 3.5 Free energies

The different ion densities in uncharged and charged electrodes are related to different free energies for ions to enter the interlayer spacing. Figure S10 shows the ionic densities for the EMIM-BF<sub>4</sub> electrolyte in contact with graphene electrodes. Free energy profiles can be extracted from these curves following:

$$G = -k_B T \ln \left( \frac{\rho(x)}{\rho_{bulk}} \right)$$

where  $k_B$  is the Boltzmann constant,  $T$  is the temperature,  $\rho(x)$  and  $\rho_{bulk}$  are the number density in the interlayer space and in the bulk respectively. Free energy profiles obtained for EMIM-BF<sub>4</sub> in contact with graphene are shown in Figure 9. Such profiles are used to extract the free energy difference between uncharged and charged states. We find that there is a significant free energy drop ( $\Delta G = -0.94 \text{ kJ.mol}^{-1}$ ) for the anion to enter in the positive interlayer space, while the energy drops for cation to enter in the positive interlayer space is smaller ( $\Delta G = -0.55 \text{ kJ.mol}^{-1}$ ).

Figure 10 gives all the free energy differences calculated in this work for the various electrode/electrolyte combinations. It is striking that cations show much larger variations of free energies than anions. This could be due, at least partly to the fact that, in the uncharged state, the electrode surfaces are either neutral or charged negatively. From the thermodynamic point of view, the free energy differences mirror what is observed in terms of proportions of intercalation / exchange / deintercalation in the charging mechanisms. When the  $\Delta G$  of cations and anions is nearly equal, the charging mechanism is mainly through ion exchange. For example, EMIM-Cl at graphene negative electrode. Otherwise, the stronger  $\Delta G$  dominates the ions migrations. For example, for EMIM-Cl at the positive graphene electrode, a more negative

$\Delta G$  of anion leads to a preferable intercalation mechanism; for EMIM-TFSI at positive  $\text{Ti}_3\text{C}_2\text{O}_2$ , a higher  $\Delta G$  of cation enhanced the deintercalation mechanism.

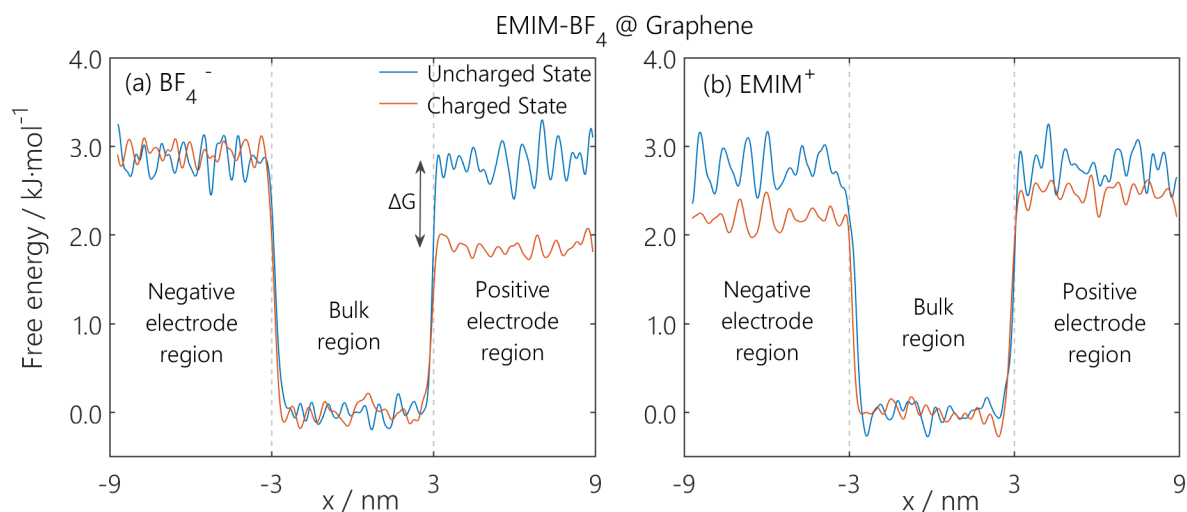


Figure 9: Free energy profiles across the simulation cell calculated for EMIM- $\text{BF}_4$  in contact with graphene electrodes. These profiles are used to determine free energy differences between charged and uncharged states.

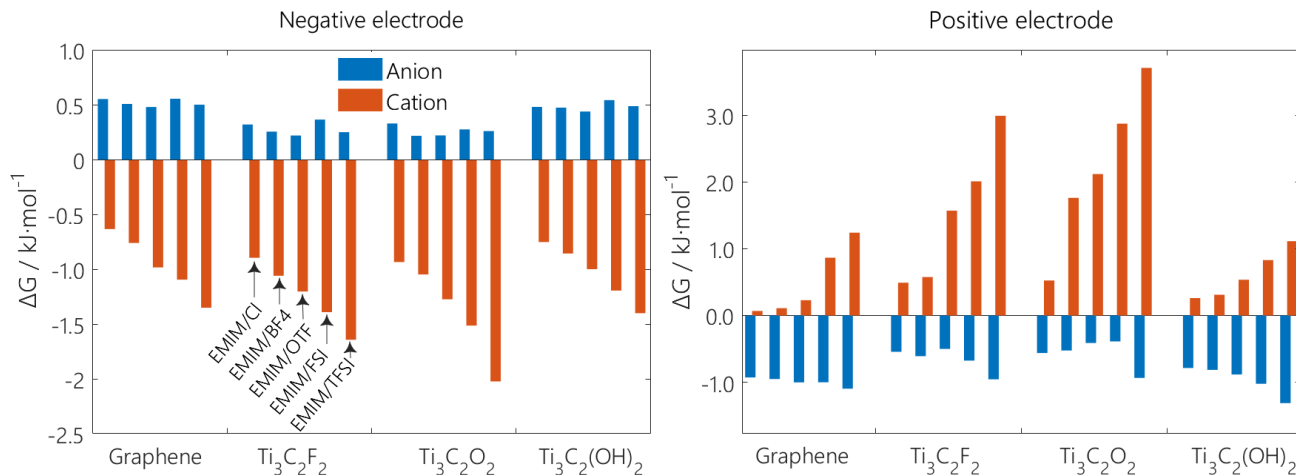


Figure 10: Comparison of calculated free energy differences,  $\Delta G$ , for all types of cations and anions entering into the negative electrode and positive electrode.

## Conclusions

Using molecular dynamics simulation methods, we conduct a systematic study of the influence of the nature of functional groups and anion size on the charging mechanisms and

volume expansion/contraction in layered materials attractive for energy storage. Typical two-dimensional material, graphene, and three different MXenes ( $\text{Ti}_3\text{C}_2\text{F}_2$ ,  $\text{Ti}_3\text{C}_2\text{O}_2$ ,  $\text{Ti}_3\text{C}_2(\text{OH})_2$ ), and five different ionic liquids are investigated. We observe that, for all electrode materials and electrolytes, the electrode expands when charged negatively and no major dependence on the anion type exists. When the electrode is charged positively, the volume changes are more complex without any specific trend following the anion size. In most cases, the volume changes can be very well interpreted using the quantities of adsorbed ions. In specific cases, e.g., for FSI<sup>-</sup> and TFSI<sup>-</sup>, the reorientation of the ions can also affect the interlayer volume. Our simulations demonstrate that the charging mechanisms (intercalation, exchange, deintercalation) are changing consistently with the anion size and are largely correlated with the surface of the electrode material in the neutral state.

Our aim was to understand the trends in the 2D layered materials charge storage mechanisms, as a function of the surface functional groups and electrolyte ion size, to provide guidance in tailoring properties of 2D layered materials for environmental and energy applications. Our simulations confirm that the nature and charge of the surface functional groups affect the charge storage mechanisms to quite a large extent. The methods employed to synthesize MXenes, which lead to different surface functional groups, thus play an important role in the final capacitive properties of the electrodes.

## Acknowledgements

This project has received funding from the European Research Council (ERC) under the European Union's Horizon 2020 research and innovation program (grant agreement no. 714581). ZL is supported by the Fundamental Research Funds for the Central Universities (YJ201886), the National Natural Science Foundation of China (Grant No. 501902215) and Sichuan Science and Technology Program (No. 2020ZDZX0005, 2020ZDZX0008). HS was supported by a grant from the China Scholarship Council (NO. 201608370077). PS, PLT and HS thank the Agence Nationale de la Recherche (Labex STORE-EX) for financial support.

## Declaration of Interest statement

The authors declare that they have no known competing financial interests or personal relationships that could have appeared to influence the work reported in this paper.

## Supplementary Material

Initial partial charges on the functional groups of MXene materials; initial and maximum charged state atomic charges for  $\text{Ti}_3\text{C}_2\text{O}_2$ ; example of net ionic charges in the interlayer spacing and standard error estimations; ion numbers in the  $\text{Ti}_3\text{C}_2\text{O}_2$  and  $\text{Ti}_3\text{C}_2(\text{OH})_2$  electrodes; interlayer and ionic volumes for the  $\text{Ti}_3\text{C}_2\text{F}_2$ ,  $\text{Ti}_3\text{C}_2\text{O}_2$  and  $\text{Ti}_3\text{C}_2(\text{OH})_2$  electrodes; EMIM<sup>+</sup> and TFSI<sup>-</sup> orientation distribution functions; proportions of charge storage mechanisms; bulk diffusion coefficients and an example of ion density profile across the simulation box are given in Supplementary Material.

## Data availability

The raw/processed data required to reproduce these findings cannot be shared at this time due to technical or time limitations.

## References

- (1) Zuo, W.; Li, R.; Zhou, C.; Li, Y.; Xia, J.; Liu, J. Battery-supercapacitor hybrid devices: recent progress and future prospects. *Adv. Sci.* **2017**, *4*, 1600539.
- (2) Zhang, L.; Hu, X.; Wang, Z.; Sun, F.; Dorrell, D. G. A review of supercapacitor modeling, estimation, and applications: A control/management perspective. *Renewable Sustainable Energy Rev.* **2018**, *81*, 1868-1878.
- (3) Wang, T.; Chen, H. C.; Yu, F.; Zhao, X.; Wang, H. Boosting the cycling stability of transition metal compounds-based supercapacitors. *Energy Storage Mater.* **2019**, *16*, 545-573.

- (4) Lin, L.; Lei, W.; Zhang, S.; Liu, Y.; Wallace, G. G.; Chen, J. Two-dimensional transition metal dichalcogenides in supercapacitors and secondary batteries. *Energy Storage Mater.* **2019**, *19*, 408-423.
- (5) Mendoza-Sánchez, B.; Gogotsi, Y. Synthesis of two-dimensional materials for capacitive energy storage. *Adv. Mater.* **2016**, *28*, 6104-6135.
- (6) Acerce, M.; Voiry, D.; Chhowalla, M. Metallic 1T phase MoS<sub>2</sub> nanosheets as supercapacitor electrode materials. *Nature Nanotech.* **2015**, *10*, 313-318.
- (7) Jun, B.-M.; Kim, S.; Heo, J.; Park, C. M.; Her, N.; Jang, M.; Huang, Y.; Han, J.; Yoon, Y. Review of MXenes as new nanomaterials for energy storage/delivery and selected environmental applications. *Nano Res.* **2019**, *12*, 471-487.
- (8) Anasori, B.; Lukatskaya, M. R.; Gogotsi, Y. 2D metal carbides and nitrides (MXenes) for energy storage. *Nat. Rev. Mater.* **2017**, *2*, 16098.
- (9) Lukatskaya, M. R.; Mashtalir, O.; Ren, C. E.; Dall'Agnese, Y.; Rozier, P.; Taberna, P. L.; Naguib, M.; Simon, P.; Barsoum, M. W.; Gogotsi, Y. Cation intercalation and high volumetric capacitance of two-dimensional titanium carbide. *Science* **2013**, *341*, 1502-1505.
- (10) Mashtalir, O.; Naguib, M.; Mochalin, V. N.; Dall'Agnese, Y.; Heon, M.; Barsoum, M. W.; Gogotsi, Y. Intercalation and delamination of layered carbides and carbonitrides. *Nature Commun.* **2013**, *4*, 1716.
- (11) Lukatskaya, M. R.; Kota, S.; Lin, Z.; Zhao, M.-Q.; Shpigel, N.; Levi, M. D.; Halim, J.; Taberna, P.-L.; Barsoum, M. W.; Simon, P.; Gogotsi, Y. Ultra-high-rate pseudocapacitive energy storage in two-dimensional transition metal carbides. *Nature Energy* **2017**, *2*, 1-6.
- (12) Come, J.; Black, J. M.; Lukatskaya, M. R.; Naguib, M.; Beidaghi, M.; Rondinone, A. J.; Kalinin, S. V.; Wesolowski, D. J.; Gogotsi, Y.; Balke, N. Controlling the actuation properties of MXene paper electrodes upon cation intercalation. *Nano Energy* **2015**, *17*, 27-35.
- (13) Zhan, C.; Sun, W.; Kent, P. R. C.; Naguib, M.; Gogotsi, Y.; Jiang, D.-e. Computational screening of MXene electrodes for pseudocapacitive energy storage. *J. Phys. Chem. C* **2019**, *123*, 315-321.

- (14) Lukatskaya, M. R.; Bak, S.-M.; Yu, X.; Yang, X.-Q.; Barsoum, M. W.; Gogotsi, Y. Probing the mechanism of high capacitance in 2D titanium carbide using *in situ* X-ray absorption spectroscopy. *Adv. Energy Mater.* **2015**, *5*, 1500589.
- (15) Wang, X.; Kajiyama, S.; Iinuma, H.; Hosono, E.; Oro, S.; Moriguchi, I.; Okubo, M.; Yamada, A. Pseudocapacitance of MXene nanosheets for high-power sodium-ion hybrid capacitors. *Nature Commun.* **2015**, *6*, 6544.
- (16) Mashtalir, O.; Lukatskaya, M. R.; Zhao, M.-Q.; Barsoum, M. W.; Gogotsi, Y. Amine-assisted delamination of Nb<sub>2</sub>C MXene for Li-ion energy storage devices. *Adv. Mater.* **2015**, *27*, 3501-3506.
- (17) Wang, X.; Mathis, T. S.; Li, K.; Lin, Z.; Vlcek, L.; Torita, T.; Osti, N. C.; Hatter, C.; Urbankowski, P.; Sarycheva, A.; Tyagi, M.; Mamontov, E.; Simon, P.; Gogotsi, Y. Influences from solvents on charge storage in titanium carbide MXenes. *Nature Ener.* **2019**, *4*, 241-248.
- (18) Lei, J.-C.; Zhang, X.; Zhou, Z. Recent advances in MXene: Preparation, properties, and applications. *Front. Phys.* **2015**, *10*, 276-286.
- (19) Li, Z.; Mendez-Morales, T.; Salanne, M. Computer simulation studies of nanoporous carbon-based electrochemical capacitors. *Curr. Opin. Electrochem.* **2018**, *9*, 81-86.
- (20) Zhan, C.; Lian, C.; Zhang, Y.; Thompson, M. W.; Xie, Y.; Wu, J.; Kent, P. R.; Cummings, P. T.; Jiang, D.-e.; Wesolowski, D. J. Computational insights into materials and interfaces for capacitive energy storage. *Adv. Sci.* **2017**, *4*, 1700059.
- (21) Lot, R.; Yilmaz, D. E.; Vlcek, L.; van Duin, A. In 2D metal carbides and nitrides (MXenes): Structure, properties and applications; Anasori, B., Gogotsi, Y., Eds.; Springer International Publishing: Cham, **2019**; pp 137-157.
- (22) Muckley, E. S.; Naguib, M.; Wang, H.-W.; Vlcek, L.; Osti, N. C.; Sacci, R. L.; Sang, X.; Unocic, R. R.; Xie, Y.; Tyagi, M.; Mamontov, E.; Page, K. L.; Kent, P. R. C.; Nanda, J.; Ivanov, I. N. Multimodality of structural, electrical, and gravimetric responses of intercalated MXenes to water. *ACS Nano* **2017**, *11*, 11118-11126.
- (23) Osti, N. C.; Naguib, M.; Ostadhossein, A.; Xie, Y.; Kent, P. R. C.; Dyatkin, B.; Rother, G.; Heller, W. T.; van Duin, A. C. T.; Gogotsi, Y.; Mamontov, E. Effect of metal ion intercalation

- on the structure of MXene and water dynamics on its internal surfaces. *ACS Appl. Mater. Inter.* **2016**, *8*, 8859-8863.
- (24) Berdiyrov, G. R.; Mahmoud, K. A. Effect of surface termination on ion intercalation selectivity of bilayer  $Ti_3C_2T_2$  (T= F, O and OH) MXene. *Appl. Surf. Sci.* **2017**, *416*, 725-730.
- (25) Xu, K.; Lin, Z.; Merlet, C.; Taberna, P.-L.; Miao, L.; Jiang, J.; Simon, P. Tracking ionic rearrangements and interpreting dynamic volumetric changes in two-dimensional metal carbide supercapacitors: A molecular dynamics simulation study. *ChemSusChem* **2018**, *11*, 1892-1899.
- (26) Jäckel, N.; Krüner, B.; Van Aken, K. L.; Alhabeb, M.; Anasori, B.; Kaasik, F.; Gogotsi, Y.; Presser, V. Electrochemical *in situ* tracking of volumetric changes in two-dimensional metal carbides (MXenes) in ionic liquids. *ACS Appl. Mater. Inter.* **2016**, *8*, 32089-32093.
- (27) Lin, Z.; Rozier, P.; Duployer, B.; Taberna, P.-L.; Anasori, B.; Gogotsi, Y.; Simon, P. Electrochemical and *in situ* X-ray diffraction studies of  $Ti_3C_2T_x$  MXene in ionic liquid electrolyte. *Electrochem. Commun.* **2016**, *72*, 50-53.
- (28) Wang, H.; Naguib, M.; Page, K.; Wesolowski, D. J.; Gogotsi, Y. Resolving the structure of  $Ti_3C_2T_x$  MXenes through multilevel structural modeling of the atomic pair distribution function. *Chem. Mater.* **2016**, *28*, 349-359.
- (29) Canongia Lopes, J. N.; Deschamps, J.; Padua, A. A. Modeling ionic liquids using a systematic all-atom force field. *J. Phys. Chem. B* **2004**, *108*, 2038-2047.
- (30) Canongia Lopes, J. N.; Pádua, A. A. H. Molecular force field for ionic liquids composed of triflate or bistriflylimide anions. *J. Phys. Chem. B* **2004**, *108*, 16893-16898.
- (31) Canongia Lopes, J. N. A.; Pádua, A. A. H. Nanostructural organization in ionic liquids. *J. Phys. Chem. B* **2006**, *110*, 3330-3335.
- (32) Connolly, M. L. Analytical molecular surface calculation. *J. Appl. Crystallogr.* **1983**, *16*, 548-558.
- (33) Plimpton, S. Fast parallel algorithms for short-range molecular dynamics. *J. Comp. Phys.* **1995**, *117*, 1-19.
- (34) Schroder, C. Comparing reduced partial charge models with polarizable simulations of ionic liquids. *Phys. Chem. Chem. Phys.* **2012**, *14*, 3089-3102.

- (35) Bowron, D. T.; D'Agostino, C.; Gladden, L. F.; Hardacre, C.; Holbrey, J. D.; Lagunas, M. C.; McGregor, J.; Mantle, M. D.; Mullan, C. L.; Youngs, T. G. A. Structure and dynamics of 1-ethyl-3-methylimidazolium acetate via molecular dynamics and neutron diffraction. *J. Phys. Chem. B* **2010**, 114, 7760-7768.
- (36) Bhargava, B. L.; Balasubramanian, S. Refined potential model for atomistic simulations of ionic liquid [BMIM][PF<sub>6</sub>]. *J. Chem. Phys.* **2007**, 127, 114510.
- (37) Chaban, V. Polarizability versus mobility: Atomistic force field for ionic liquids. *Phys. Chem. Chem. Phys.* **2011**, 13, 16055-16062.
- (38) Cao, Y.; Mu, T. Comprehensive investigation on the thermal stability of 66 ionic liquids by thermogravimetric analysis. *Ind. Eng. Chem. Res.* **2014**, 53, 8651-8664.
- (39) Efimova, A; Pfützner, L.; Schmidt, P. Thermal stability and decomposition mechanism of 1-ethyl-3-methylimidazolium halides. *Thermochim. Acta* **2015**, 604, 129-136.
- (40) Liu, Z.; El Abedin, S. Z.; Endres, F. Electrochemical and spectroscopic study of Zn(II) coordination and Zn electrodeposition in three ionic liquids with the trifluoromethylsulfonate anion, different imidazolium ions and their mixtures with water. *Phys. Chem. Chem. Phys.* **2015**, 17, 15945-15952.
- (41) Ishikawa M.; Sugimoto T.; Kikuta, M.; Ishiko, E; Kono, M.. Pure ionic liquid electrolytes compatible with a graphitized carbon negative electrode in rechargeable lithium-ion batteries. *J. Power Sources* **2006**, 162, 658-662.
- (42) Xu, K.; Ji, X.; Zhang, B.; Chen, C.; Ruan, Y.; Miao, L.; Jiang, J. Charging/discharging dynamics in two-dimensional titanium carbide (MXene) slit nanopore: Insights from molecular dynamic study. *Electrochim. Acta* **2016**, 196, 75-83.
- (43) Merlet, C.; Péan C.; Rotenberg, B.; Madden, P. A.; Simon, P.; Salanne M. Simulating supercapacitors: Can we model electrodes as constant charge surfaces? *J. Phys. Chem. Lett.* **2013**, 4 264-268.
- (44) Wang, Z.; Yang, Y.; Olmsted, D. L.; Asta, M.; Laird, B. B. Evaluation of the constant potential method in simulating electric double-layer capacitors. *J. Chem. Phys.* **2014**, 141, 184102.

- (45) Liu, Y. M.; Merlet, C.; Smit, B. Carbons with regular pore geometry yield fundamental insights into supercapacitor charge storage, *ACS Cent. Sci.* **2019**, *5*, 1813-1823.
- (46) Hantel, M.; Presser, V.; Kotz, R.; Gogotsi, Y. *In situ* electrochemical dilatometry of carbide-derived carbons. *Electrochem. Commun.* **2011**, *13*, 1221-1224.
- (47) Hantel, M. M.; Presser, V.; McDonough, J. K.; Feng, G.; Cummings, P. T.; Gogotsi, Y.; Kotz, R. *In situ* electrochemical dilatometry of onion-like carbon and carbon black. *J. Electrochem. Soc.* **2012**, *159*, A1897-A1903.
- (48) Hantel, M.; Weingarth, D.; Kotz, R. Parameters determining dimensional changes of porous carbons during capacitive charging. *Carbon* **2014**, *69*, 275-286.
- (49) Kaasik, F.; Tamm, T.; Hantel, M. M.; Perre, E.; Aabloo, A.; Lust, E.; Bazant, M. Z.; Presser, V. Anisometric charge dependent swelling of porous carbon in an ionic liquid. *Electrochem. Commun.* **2013**, *34*, 196-199.
- (50) Forse, A. C.; Merlet, C.; Griffin J.; Grey. C. P. New perspectives on the charging mechanisms of supercapacitors. *J. Am. Chem. Soc.* **2016**, *138*, 5731-5744.
- (51) Péan, C; Rotenberg, B.; Simon, P.; Salanne, M. Understanding the different (dis)charging steps of supercapacitors: influence of potential and solvation. *Electrochim. Acta* **2016**, *206*, 504-512.
- (52) Noh, C., N.; Jung, Y. Understanding the charging dynamics of an ionic liquid electric double layer capacitor via molecular dynamics simulations. *Phys. Chem. Chem. Phys.* **2019**, *21*, 6790-6800.
- (53) Kowsari, M. H; Alavi, S.; Ashrafizaadeh, M.; Najafi, B., Molecular dynamics simulation of imidazolium-based ionic liquids. I. Dynamics and diffusion coefficient. *J. Chem. Phys.* **2008**, *129*, 224508.
- (54) Holbrey, J. D.; Rogers, R. D.; Mantz, R. A.; Trulove, P. C.; Cocalia, V. A.; Visser, A. E.; Anderson, J. L.; Anthony, J. L.; Brennecke, J. F.; Maginn, E. J.; Welton, T.; Mantz, R. A., *Ionic Liquids in Synthesis*. Wiley **2008**, Chapter 3 - Physicochemical Properties, 57-174.
- (55) Tokuda, H.; Hayamizu, K.; Ishii, K.; Susan, Md. A. B. H.; Watanabe, M.; Physicochemical Properties and Structures of Room Temperature Ionic Liquids. 2. Variation of Alkyl Chain Length in Imidazolium Cation. *J. Phys. Chem. B* **2005**, *109*, 6103-6110.